NPC Natural Product Communications

2014
Vol. 9
No. 8
1087 - 1090

Mechanistic Studies on the Intramolecular Cyclization of *O*-Tosyl Phytosphingosines to Jaspines

Ramón Crehuet[a], David Mormeneo[b,c], Josep M. Anglada[a,*] and Antonio Delgado[b,c,*]

[a]*Theoretical and Computational Chemistry Group, IQAC-CSIC, c/ Jordi Girona 18-26, E-08034 Barcelona, Spain*
[b]*Unitat de Química Farmacèutica (Unitat Associada al CSIC), Facultat de Farmàcia, Universitat de Barcelona (UB), Avgda. Juan XXIII, s/n, 08028 Barcelona, Spain*
[c]*Departament de Química Biomèdica; Research Unit on BioActive Molecules (RUBAM), IQAC-CSIC, Jordi Girona 18-26, 08034 Barcelona, Spain*

anglada@iqac.csic.es; antonio.delgado@ub.edu

Received: April 16th, 2014; Accepted: May 16th, 2014

A theoretical study to elucidate the mechanistic aspects involved in the tosylation-cyclization reaction of diastereomeric phytosphingosines **1a-1d** to jaspines **4a-4d** is presented. The stereochemistry of the starting stereoisomers is crucial for the development of weak interactions, both in the reactants and in the transition states. The analysis of the energy barriers of each elementary reaction is consistent with the observed reluctance of tosylate **2d** to undergo cyclization. In addition, the initial tosylation can be identified as the limiting step in cyclizations from **1a** and **1b.**

Keywords: Ab-initio calculations, Cyclization, Reaction mechanisms, Sphingolipids, Jaspine B.

Jaspine B (pachastrissamine) is a cytotoxic marine natural product isolated in 2002 from the sponge *Jaspis* sp.[1] The interesting biological properties of this anhydrophytosphingosine has prompted chemists to develop a variety of synthetic methodologies leading to both the natural compound and analogues thereof. [2,3] In the course of our research on sphingolipid analogues, we reported the total synthesis and cytotoxic properties of natural jaspine B. In the same work, diastereomeric jaspines arising from the formal stereochemical inversion of C3 and/or C4 stereogenic centers of the natural product were also reported (Figure 1). [4] Our synthetic approach relied on the intramolecular one-pot tosylation-cyclization of stereochemically defined *N*-Boc phytosphingosines **1a-d** (Scheme 1). However, the reaction outcome was strongly dependent on the stereochemisty of the starting compounds. Intrigued by this finding, we undertook a theoretical study aimed at deciphering the structural and/or electronic parameters involved in these processes. The results of this research are presented in this work.

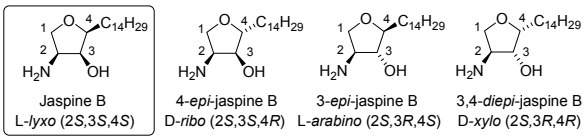

Figure 1: Jaspine B and diastereomeric jaspines synthesized in our group.

Intramolecular tosylation-cyclization of stereochemically defined *O*-tosyl-*N*-Boc phytosphingosines **1a-d** was carried out as shown in Scheme 1 and Table 1. The standard cyclization protocol requires an excess of TsCl (3 equiv/mol) and TEA (5 equiv/mol) in the presence of cat DMAP in CH_2Cl_2 at rt (Table 1).

Interestingly, while cyclization took place uneventfully from **1a** and **1c**, presumably through the participation of transient tosylates **2a** and **2c**, [5] the same reaction conditions were less efficient from **1b** (entry 2), where recovered starting material was the major product, and they totally failed from **1d** (entry 4), where tosylate **2d** was isolated in acceptable yields (66%). However, tosylate **2d** could be cyclized to **4d** following an alternative protocol, as described in the literature (K_2CO_3, MeOH, 20 h, 0-25ºC) [7].

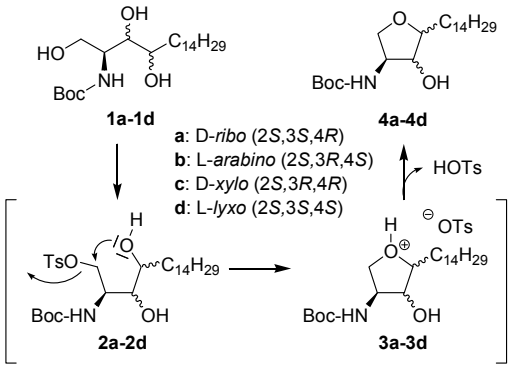

Scheme 1: Intramolecular cyclization leading to *N*-Boc jaspines. Conditions: TsCl (3 equiv/mol), TEA (5 equiv/mol), DMAP (cat), CH_2Cl_2, 25ºC, 6 h.

Table 1: Cyclization of *N*-Boc phytosphingosines **1a-1d** to *N*-Boc jaspines **4a-4d** (see Scheme 1).

Entry	Starting material	Cyclization product (%) [a]	Other (%)
1	**1a** (D-*ribo*)	**4a** (56)	**1a** (10)
2	**1b** (L-*arabino*)	**4b** (19)	**1b** (65)
3	**1c** (D-*xylo*)	**4c** (58)	-----
4	**1d** (L-*lyxo*)	**4d** (--)	**1d** (16) **2d** (66) [b]

a) See Scheme 2 b) See ref [6].

The different yields in the cyclization products **4a-4d** (Table 1) led us to investigate the reaction course from the putative intermediate tosylates **2a-2d**. To this end, we have carried out a theoretical study considering the elementary reaction leading to the formation of intermediates **3a-3d** from **2a-2d**. These reactions involve a formal S_N2 process, followed by the subsequent deprotonation of intermediates **3a-3d**. The process has been modelled from the corresponding sulfonate surrogates **2'a-2'd**, as shown in Scheme 2. For computational purposes, the large $C_{14}H_{29}$ alkyl side chain, the tosyl group and the bulky Boc group were replaced with the smaller methyl, mesyl and methoxycarbonyl groups, respectively, as these groups are not expected to have a major influence on the particular reactivity observed for the different diastereoisomers considered in this work.

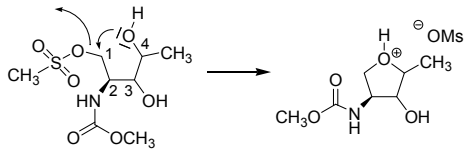

2'a: D-*ribo* (2*S*,3*S*,4*R*)
2'b: L-*arabino* (2*S*,3*R*,4*S*)
2'c: D-*xylo* (2*S*,3*R*,4*R*)
2'd: L-*lyxo* (2*S*,3*S*,4*S*)

3'a-3'd

Scheme 2: Sulfonate surrogates **2'a-2'd** and the modelled cyclization reaction to **3'a-3'd**.

The large flexibility of models **2'a-2'd** prompted us to consider the most stable conformers for each diastereoisomer. For this reason, a simulated annealing (SA) process to obtain the most stable conformer for each minima and transition state was carried out first. A DFT method with the B3LYP functional to locate and characterize each stationary point was used next. Finally, the solvation effects using the PCM approach were also considered. An energy profile pointing out the relative energy position of the reactants and transition states is shown in Figure 2, whereas the most relevant geometrical parameters of the most stable conformers of the reactants **2'** and the transition states connecting **2'** to **3'** are plotted in Figure 3. It is remarkable that the transition states are not generated from the absolute minima, because the most stable minima need not be connected with the lowest transition states. The located transition states are connected with conformations that are above the lowest minima, but in fast equilibrium with them.

The results displayed in Figure 2 and Table 2 show that the computed energy barriers at gas phase ($\Delta E^{\ddagger\ gas}$, Table 2) range between 32.2 and 38.8 kcal/mol. However, consideration of the solvation effects diminishes the barrier heights, so that our calculations in solution ($\Delta G^{\ddagger\ sol}$, Table 2) predict free energy barriers of 22.4 (for **2'b** to **3'b**) and 21.3 (for **2'c** to **3'c**) kcal/mol, a slightly larger energy barrier (24.3 kcal/mol) for the **2'a** to **3'a** process and a quite larger energy barrier (30.8 kcal/mol) for the **2'd** to **3'd** process.

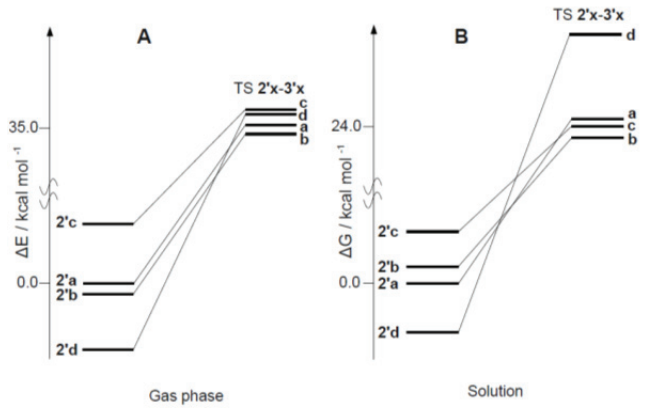

Figure 2: Energy profile of the relative energy position of the reactants and transition states in the process **2'-3'**.

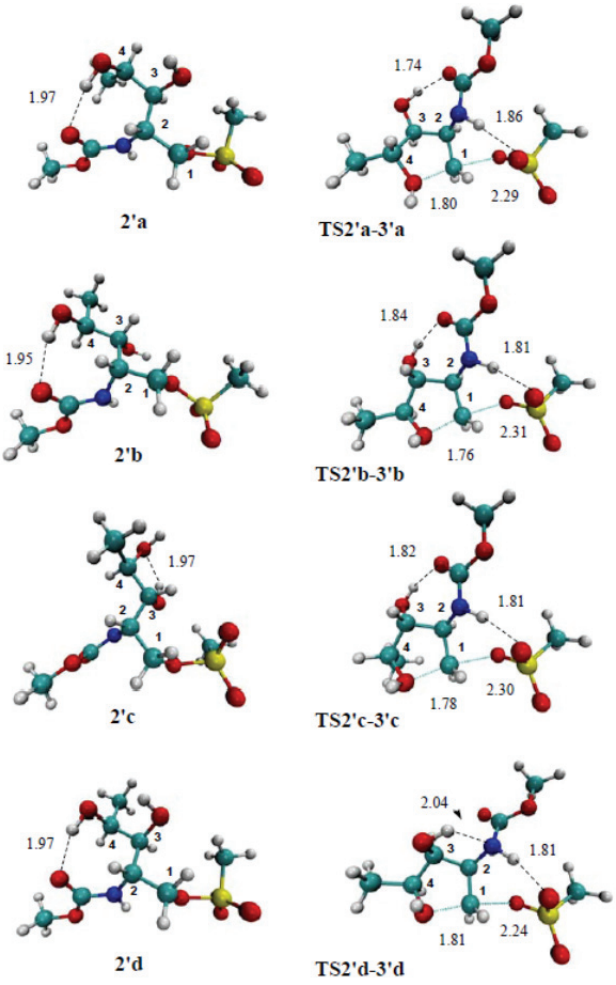

Figure 3: Geometries of the most stable conformers of the reactants **2'** and the transition states connecting **2'** to **3'**. Dotted lines stand for hydrogen bond interactions. The numbers are the hydrogen bond lengths, in Angstroms.

A detailed analysis of our calculations shows that the computed barrier heights are the result of different effects. Thus, the results displayed in Table 2 and Figure 2A for the gas phase already predict the higher energy barrier (around 6 kcal/mol) for the **2'd-3'd** reaction, pointing out the involvement of different internal contributions to the stability of the reactants **2'**. A closer look at the geometries of the reactants and transition states (Figure 3) indicates that the spatial arrangement of the substituents for each diastereomer allows the development of different weak interactions on the corresponding stationary points, which play a fundamental role in their relative stabilization. Thus, for instance, reactants **2'a**, **2'b** and **2'd** show a hydrogen bond between C4(OH) and the carbamate CO carbonyl, whereas in **2'c** a hydrogen bond between C3(OH) and C4(OH) is observed. Since OH-OH hydrogen bonds are weaker than OH-O=C bonds [8] **2'c** is destabilized by about 3 kcal/mol with respect to the remaining reactants (see Figure 2a).

Table 2: Computed energy barriers at gas phase and in solution (CH_2Cl_2).

Entry	Reaction	$\Delta E^{\ddagger\ gas}$	$\Delta G^{\ddagger\ sol}$	$\Delta\Delta G_M$	$\Delta\Delta G_{TS\text{-}TS}$	k (298K)	τ (298K)
1	**2'a-3'a**	34.4	24.3	0.0	0.0	$9.44\cdot10^{-6}$	29.4
2	**2'b-3'b**	34.2	22.4	0.9	-1.0	$2.22\cdot10^{-4}$	1.3
3	**2'c-3'c**	32.2	21.3	2.6	-0.4	$1.53\cdot10^{-3}$	0.3
4	**2'd-3'd**	38.8	30.8	-2.4	4.1	$1.52\cdot10^{-10}$	$1.8\cdot10^{-6}$

$\Delta E^{\ddagger\ gas}$ is the potential energy barrier in gas phase; $\Delta G^{\ddagger\ sol}$ is the free energy barrier in solution;. $\Delta\Delta G_M$ is the free energy difference between compounds **2'**and **2'a** in solution; $\Delta\Delta G_{TS\text{-}TS}$ is the free energy difference between all the transition states with respect to the transition state for **2'a-3'a** in solution; k is the unimolecular rate constant (in s^{-1}) computed at 298K and τ is the reaction time (in h).

Regarding the transition states, all of them have similar energies at the gas phase. Thus, **TS2'c-3'c** is destabilized by less than 1.0 kcal/mol with respect to **TS2'a-3'a** (Figure 2A). This is in agreement with their geometry, where two hydrogen bond interactions can be observed in each case (SO···HN and OH···O=C for **TS2'a-3'a**; **TS2'b-3'b** and **TS2'c-3'c** and SO···HN and OH···N for **TS2'd-3'd**), see Figure 3. Consequently, all transition states are similarly stabilized as a result of the hydrogen bond interactions. Finally, the results displayed in Table 2 and Figure 2B show that the contribution of the solute-solvent electrostatic interactions in the solvation model adds more bias to the relative energetic position of the different stationary points. Thus, for instance, the $\Delta\Delta G_M$ values from Table 2 show that **2'c** is destabilized by 2.6 kcal/mol with respect to **2'a**, but **2'd** is stabilized by 2.4 kcal/mol with respect to **2'a**, whereas the $\Delta\Delta G_{TS\text{-}TS}$ shows that the $\mathbf{TS_{2'd\text{-}3'd}}$ is destabilized by 4.1 kcal/mol with respect to $\mathbf{TS_{2'a\text{-}3'a}}$. As a result of all differential effects occurring in the gas phase and in solution, there is a difference of 9.5 kcal/mol (30.8-21.3 kcal/mol, see Table 2) in the computed free energy barriers between the most favourable (**2'c-3'c**) and the most unfavourable (**2'd-3'd**) processes.

The computed free energy barriers displayed in Table 2 allowed us to estimate the corresponding rate constants (k_v) and, consequently, the reaction times (τ) by application of conventional transition state theory (equation 1)

$$k_v = \frac{1}{\tau} = \frac{k_b T}{h} e^{\frac{-(\Delta G^{\ddagger})}{RT}} \quad (1)$$

where $\Delta G^{\ddagger}$ is the free energy difference of the reactants and the transition state, k_b, h and R are the Boltzmann, Planck, and universal gas constants, and T is the temperature. The corresponding results are also displayed in Table 2 and suggest that one would expect a fast formation of compounds **4b** and **4c**, a slower formation of compound **4a**, and an almost insignificant formation of compound **4d** from their corresponding intermediate tosylates **2a-2d**. This is consistent with the experimental observations displayed in Table 1 for **4a** and **4c**, which are formed in acceptable yields, and also for **4d**, whose formation was not observed at the expense of tosylate **2d**, which became the major reaction product from **1d** (Table 1, entry 4). Since these results are not consistent with the small amounts of **4b** (see Table 1), we have also taken into account the different yields in the cyclization products in an attempt to clarify this discrepancy. Thus, unreacted starting material **1** was recovered in all cases, with the exception of **1c** (Table 1, entry 3). However, reaction from **1b** (entry 2) was especially relevant, since the starting material was the major product and the corresponding jaspine diastereomer **4b** was obtained in low yield, despite the expected high cyclization rate predicted by our calculations (Table 2, entry 2). This result can be rationalized by assuming that tosylation is the rate limiting step from **1b**, which prevents the formation of **2b** and the subsequent cyclization process. The same holds true for **1a**, where a small amount of starting material was recovered with no trace of intermediate tosylate **2a** (Table 1, entry 1), despite the calculated lower rate constant for the **2a**→**3a** cyclization step (Table 2, entry 1). These results point out the dramatic effect of the tosylation step in this one-pot two-step cyclization. A full clarification of this point would require a further theoretical study on the tosylation of **1**, which is beyond the scope of the present work. The continuum solvation models used in the present work can describe neither the explicit participation of solvent molecules that are presumably involved in the toluensulfonate esterification, nor the pH-effects in a reaction where HCl is produced.

In summary, we have performed a joint experimental and theoretical study aiming at elucidating the mechanistic aspects of the cyclization step in the formation of the *N*-Boc jaspines **4a-4d**. The calculations show that the stereochemistry of the different stereoisomers on the starting triols **1a-1d** is crucial for the development of weak interactions, such as hydrogen bonds and/or solute-solvent effects, both in the reactants and in the transition states. These interactions play an important role in the height of the energy barriers of each elementary reaction and satisfactorily explain the reluctance of intermediate tosylate **2d** to undergo cyclization to jaspine **4d**. In addition, by combination of experimental and theoretical results, the initial tosylation can be identified as the limiting step in cyclizations from **1a** and **1b**.

Computational details: To obtain the lowest conformer of each transition state, we began by locating a conformer of the transition state of each diastereoisomers employing the B3LYP functional.

The simulated annealing (SA) cycles were made with the RM1 semi-empirical Hamiltonian 10. SA cycles were performed consisting of 200ps of heating time from 0 to 2500K, followed by 100ps of cooling to 100K and a final conjugate gradient optimization. For the sake of completeness, when the lowest conformation for each of the diastereomers was found, the equivalent diastereomeric conformation was modelled by hand and optimized following the described procedure in order to ensure that it had not been missed by the SA. In all cases the resulting conformation had larger energy than the one found by the SA, proving that the SA cycle was long enough. The search for transition states follows a similar procedure. First, a transition state for the reaction from **3** to **4** was located with B3LYP/6-31G(d). Then, for each of the molecules **4a**-**4d** a series of SA was performed analogous to the that previously described, but including an harmonic constrain (2500 kJ/A^2) to restrain the bonds that were being formed and cleaved. Finally, these structures were used as initial guesses to optimize the geometry of the transition state with B3LYP/6-31G(d) without constraints in the gas-phase. The final energies were obtained by performing single point energy calculations at the optimized geometries, at the B3LYP/6-311+G(2df,2p) level of theory. The energy in solution was obtained from single point energy calculations with the polarized continuum method (PCM) approach. The SA and the DFT calculations were performed with the Dynamo library [9] and Gaussian 03 program, [10], respectively. The bonding features have been analyzed by using the atoms in molecules (AIM) theory by Bader [11] with the AIMPAC program. [12]

Supplementary data: Contains Cartesian coordinates and absolute energies of the stationary points investigated.

Acknowledgments - Financial support from Generalitat de Catalunya (Grants 2009SGR1072 and 2009SGR1472) is acknowledged. The calculations described in this work were carried out at the Centre de Supercomputació de Catalunya (CESCA) and the CTI-CSIC. D.M. acknowledges the Ministerio de Educación y Ciencia, Spain, for a predoctoral fellowship.

References

[1] Ledroit V, Debitus C, Lavaud C, Massiot G. (**2003**) Jaspines A and B: Two new cytotoxic sphingosine derivatives from the marine sponge *Jaspis* sp. *Tetrahedron Letters*, ***44***, 225–228.

[2] For recent synthetic approaches to jaspine B and analogs, see: (a) Dhand V, Chang S, Britton R. (**2013**) Synthesis of pachastrissamine (jaspine B) and its derivatives by the late-stage introduction of the C-2 alkyl side-chains using olefin cross metathesis. *Journal of Organic Chemistry*, ***78***, 8208–8213; (b) Ghosal P, Ajay S, Meena S, Sinha S, Shaw AK. (**2013**) Stereoselective total synthesis of Jaspine B (Pachastrissamine) utilizing iodocyclization and an investigation of its cytotoxic activity. *Tetrahedron: Asymmetry*, ***24***, 903–908; (c) Jana AK, Panda G. (**2013**) Stereoselective synthesis of Jaspine B and its C2 epimer from Garner aldehyde. *Royal Society of Chemistry Advances,* ***3***, 16795–16801; (d) Martinkova M, Pomikalova K, Gonda J, Vilkova M. (**2013**) A common approach to the total synthesis of L-arabino-, L-ribo-C18-phytosphingosines, ent-2-epi-jaspine B and 3-epi-jaspine B from D-mannose. *Tetrahedron*, ***69***, 8228–8244; (e) Santos C, Fabing I, Saffon N, Ballereau S, Genisson Y. (**2013**) Rapid access to jaspine B and its enantiomer. *Tetrahedron*, ***69***, 7227–7233; (f) Yoshimitsu Y, Miyagaki J, Oishi S, Fujii N, Ohno H. (**2013**) Synthesis of pachastrissamine (jaspine B) and its derivatives by the late-stage introduction of the C-2 alkyl side-chains using olefin cross metathesis. *Tetrahedron*, ***69***, 4211–4220; (g) Srinivas Rao G, Chandrasekhar B, Venkateswara Rao B. (**2012**) Total synthesis of the acetyl derivatives of lyxo-(2R,3R,4R)-phytosphingosine and (−)-jaspine B. *Tetrahedron: Asymmetry*, ***23***, 564–569; (h) Zhao M-L, Zhang E, Gao J, Zhang Z, Zhao Y-T, Qu W, Liu H-M. (**2012**) An efficient and convenient formal synthesis of Jaspine B from D-xylose. *Carbohydrate Research* ***351***, 126–129.

[3] Delgado A, Fabriàs G, Casas J, Abad JL. (**2013**) Natural products as platforms for the design of sphingolipid-related anticancer agents. *Advances in Cancer Research*, ***117***, 237–281.

[4] Canals D, Mormeneo D, Fabriàs G, Llebaria A, Casas J, Delgado A. (**2009**) Synthesis and biological properties of pachastrissamine (jaspine B) and diastereoisomeric jaspines. *Bioorganic and. Medicinal Chemistry*, ***17***, 235–241.

[5] Van den Berg RJ, Boltje TJ, Verhagen CP, Litjens RE, van der Marel GA, Overkleeft HS. (**2006**) An efficient synthesis of the natural tetrahydrofuran pachastrissamine starting from D-ribo-phytosphingosine. *Journal of. Organic Chemistry,* ***71***, 836–839.

[6] Compound **5** was obtained in 13% yield.

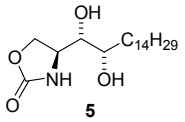

5

Formation of **5** can be interpreted as a result of an intramolecular displacement of the tosyloxy group in **2d** by the carbonyl group of the carbamate moiety..

[7] Ribes C, Falomir E, Carda M, Marco JA. (**2006**) Stereoselective synthesis of pachastrissamine (jaspine B). *Tetrahedron*, ***62***, 5421–5425.

[8] Torrent-Sucarrat M, Anglada JM. (**2006**) On the gas phase hydrogen bond complexes between formic acid and hydroperoxyl radical. A theoretical study. *Journal of Physical Chemistry A*, ***110***, 9718–9726.

[9] Field MJ, Albe M, Bret C, Proust-De Martin F, Thomas A. (**2000**) The dynamo library for molecular simulations using hybrid quantum mechanical and molecular mechanical potentials. *Journal of Computational Chemistry*, ***21***, 1088–1100.

[10] Gaussian 03, Revision C.01, Frisch MJ, Trucks GW, Schlegel HB, Scuseria GE, Robb MA, Cheeseman JR, Montgomery Jr. JA, Vreven T, Kudin KN, Burant JC, Millam JM, Iyengar SS, Tomasi J, Barone V, Mennucci B, Cossi M, Scalmani G, Rega N, Petersson GA, Nakatsuji H, Hada M, Ehara M, Toyota K, Fukuda R, Hasegawa J, Ishida M, Nakajima T, Honda Y, Kitao O, Nakai H, Klene M, Li X, Knox JE, Hratchian HP, Cross JB, Bakken V, Adamo C, Jaramillo J, Gomperts R, Stratmann RE, Yazyev O, Austin AJ, Cammi R, Pomelli C, Ochterski JW, Ayala PY, Morokuma K, Voth GA, Salvador P, Dannenberg JJ, Zakrzewski VG, Dapprich S, Daniels AD, Strain MC, Farkas O, Malick DK, Rabuck AD, Raghavachari K, Foresman JB, Ortiz JV, Cui Q, Baboul AG, Clifford S, Cioslowski J, Stefanov BB, Liu G, Liashenko A, Piskorz P, Komaromi I, Martin RL, D. Fox DJ, Keith T, Al-Laham MA, Peng CY, Nanayakkara A, Challacombe M, Gill PMW, Johnson B, Chen W, Wong MW, Gonzalez C, Pople JA. (**2004**) Gaussian, Inc., Wallingford CT.

[11] Bader RFW. (**1990**) *Atoms in Molecules. A Quantum Theory*. Clarendon Press, Oxford, U.K..

[12] Bader RFW. Accessed May 2002 ed., http://www.chemistry.mcmast.